Study on the Material Model and Hot Working Drawing of a New Type of High Temperature Titanium Alloy Ti-Al-Nb

Shuang Fang*, *Mincong* Zhang, *Qiuying* Yu and *Huaping* Xiong

Beijing Institute of Aeronautical Materials, Beijing, 100095, China.

Abstract. This paper proposes an exploratory study on the preparation of titanium-based superalloys through the Ti+Al+Ti2AlNb three-component hybrid hot press sintering method. Through the hot press sintering experiment of the mixed powder under different heating and sintering processes, the plastic deformation behavior of the material is carried out on this basis Research, preliminarily discuss the constitutive relationship of the new high-temperature titanium alloy Ti-Al-Nb, establish the hot working map and recrystallization model.

1 Introduction

As a light metal structural material with good comprehensive performance, titanium alloy has been widely used in aviation, aerospace and other fields. However, as the temperature rises, the oxidation resistance and high temperature strength of titanium alloys are significantly reduced, which greatly limits the maximum use temperature. At present, the working temperature of advanced heat-resistant titanium alloys only reaches 550°C~600°C[1-3] . Therefore, research on high temperature titanium alloys above 600°C has always been a development trend in the field of titanium alloy materials.

This paper proposes an exploratory study on the preparation of titanium-based superalloys through the Ti+Al+Ti2AlNb three-component hybrid hot-press sintering method. It is planned to conduct hot-press sintering experiments of mixed powders under different hot-press sintering processes, and carry out the plasticity of the material on this basis. Deformation behavior research, preliminary discussion of the constitutive relationship of the new high-temperature titanium alloy Ti-Al-Nb, establishment of hot working diagrams and recrystallization models, laying a technical foundation for the development of a new type of high-temperature titanium-based alloy with low brittleness at room temperature.

* Corresponding author: fs107114@126.com

2 Experimental

The raw materials used in the experiment are pure Ti powder, pure Al powder and Ti2AlNb alloy powder. The powder is produced by Xi'an Ouzhong Material Technology Co., Ltd. The chemical composition of the raw material powder used in the test is listed in Table 1.

Table 1. Chemical composition of pure Ti, Al and Ti2AlNb powder (wt%)

Element	Fe	C	O	N	H	Ti	/	Ti
Content, wt%	0.023	0.023	0.1661	0.0066	0.0023	Bal	/	
Element	Ti	O	Zn	Cu	Fe	Si	Al	Al
Content, wt%	<0.01	0.096	<0.01	<0.01	<0.01	<0.01	Bal	
Element	Al	Nb	C	N	O	H	/	Ti2AlNb
Content, wt%	10.25	42.90	0.008	0.002	0.068	0.002	/	

Through scanning electron microscopy secondary electron imaging, it is observed that the raw material powder used in the experiment is spherical particles of nearly equal diameter. As shown in Figure 1, The 400 mesh pure Ti powder has a relatively uniform particle size distribution. The 400 mesh pure Al powder has smaller spherical particles agglomerated near the 400 mesh powder particle size particles, and the 400 mesh Ti2AlNb alloy powder has smaller size spherical particles agglomerated near the 400 mesh powder particle size particles. Particles.

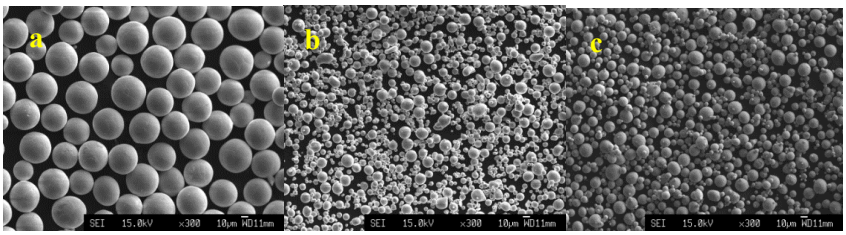

Fig. 1. SEM photo of the raw material powder (400 mesh) used in the experiment (a)pure Ti powder; (b)pure Al powder; (c)Ti2AlNb alloy powder;

Based on the hot pressing sintering process, hot pressing sintered crystal grain growth kinetics and hot pressing sintering densification kinetics, the mixing ratio of raw material powder and the hot pressing sintering system are designed (Table 2).

Table 2. Mixing ratio of raw material powder and hot pressing sintering system

Num	Ti_2AlNb proportion	mesh	Hot pressing sintering system		
			Temperature°C	Press, MPa	Time, h
4#	5%	400	1200	30	1.5
5#	10%				
6#	15%				
7#	10%		1400		1.5
8#			1300		
9#			1200		3
10#					4.5
11#	5%		1250		1.5
12#	10%				
13#	15%				
14#	5%		1300		
15#	15%				

Weigh the pure Ti powder and pure Al powder according to the volume ratio of 1:1, then weigh the Ti2AlNb powder according to the Ti2AlNb powder ratio in Table 2, and put the weighed three raw material powders into a mortar and mix them thoroughly. Put the mixed raw materials into a graphite mold. The inner size of the graphite mold is Φ60mm×40mm. The inner wall of the graphite mold, graphite paper and graphite sheet are uniformly coated with boron nitride in advance, and placed in an oven to dry to prevent sintering Carbon pick-up occurs during the process, resulting in sticky molds. Put the loaded graphite mold into a vacuum hot-pressing sintering furnace. First, pre-press the graphite mold to a pressure of 30MPa, and then release the pressure; secondly, vacuumize the vacuum hot-pressing sintering furnace and pass argon gas into it. Vacuum a second time, let in argon gas, and then start to increase the temperature at a rate of 10°C/s. The pressure is maintained at 30 MPa from the temperature rise to the completion of sintering, and wait until the temperature reaches the corresponding hot pressing sintering temperature (1200°C to 1400°C)), keep the corresponding time (1.5h ~ 4.5h), stop heating and depressurize, the alloy billet is cooled to room temperature along with the furnace.

The sample size of the uniaxial compression deformation test is Φ10 × 15mm. The true stress-true strain curve of the deformation test is shown in Figure 1.

3 Results and Discussion

Figure 2 is the true stress-true strain curve of the new type of titanium aluminum material in the high temperature uniaxial compression deformation process under the conditions of deformation temperature of 1000~1100°C, deformation rate of 0.001~1s-1, and strain value of 0.9. Under the conditions of deformation temperature and deformation rate, the basic common feature is [4-5]: as the strain value increases, the flow stress increases rapidly, and the minimum stress value and corresponding strain required for recrystallization to start nucleation are first broken. After that, the flow stress continues to rise until it reaches a peak value, and the corresponding stress and strain values are the peak stress σp and the peak strain εp; after this peak strain εp, with As the strain value increases, the flow stress shows a certain decreasing trend until it reaches a minimum value. The corresponding stress and strain values are steady-state stress σss and steady-state strain εss. After a certain degree of strain accumulation, the flow stress The stress continues to increase as the strain value continues to increase, and this trend of increase continues to the final strain value of the experimental design. The corresponding stress value is defined as the end stress σfinal, and the corresponding strain value is 0.9.

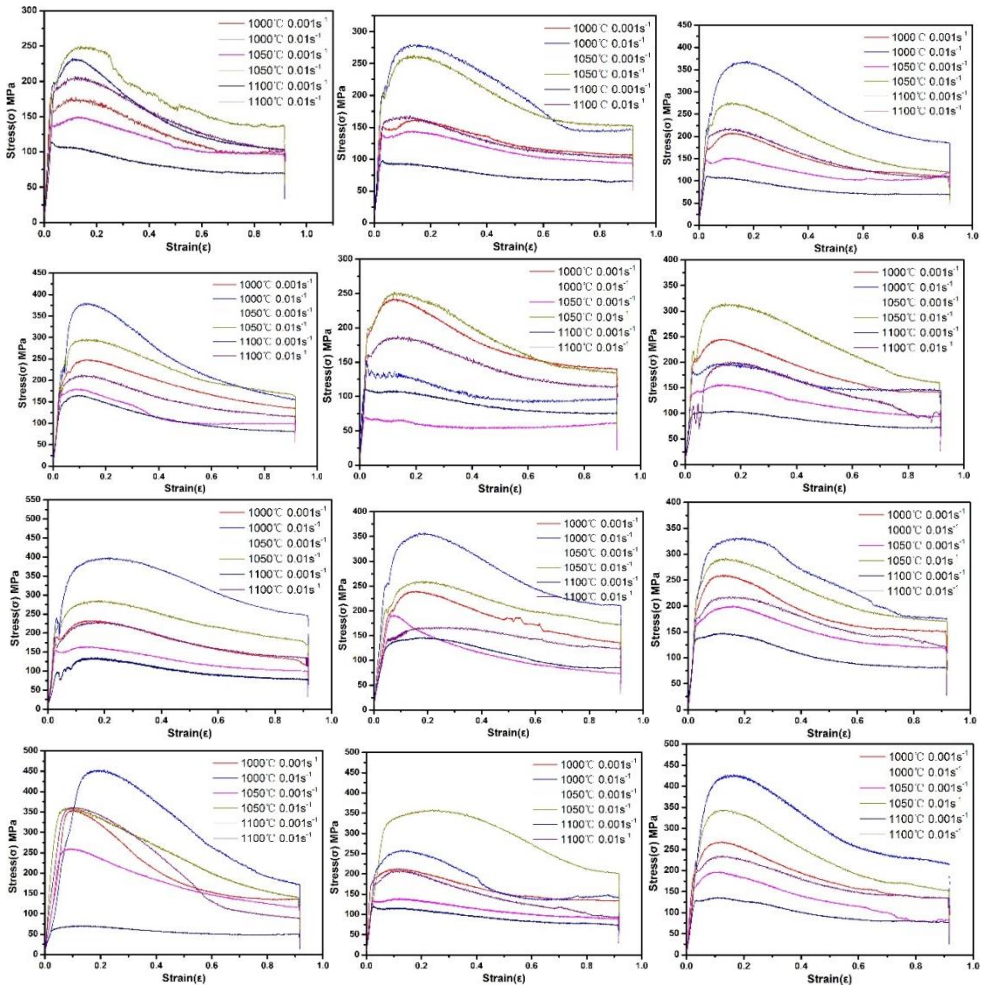

Fig. 2. The true stress-true strain curve of a new type of titanium-aluminum material under uniaxial compression

The thermal deformation of metals and alloys is a thermal activation process. The relationship between flow stress σ, temperature T and strain rate is usually analyzed by different forms of Arrhenius equation[6]:

$$A_1 \exp(\beta\sigma) = Z \tag{1}$$

$$A_2 \sigma^{n_1} = Z \tag{2}$$

$$A_3 [\sinh(\alpha\sigma)]^{n_2} = Z \tag{3}$$

Where: σ is the flow stress (MPa); A1, A2, A3 and β, n1, n2 are the material constants; α is the stress adjustment coefficient, at a constant temperature, and ln[sinh(ασ)] keep parallel Linear relationship, α, β and n1 satisfy the relationship; Z is the Zener-Hollmon parameter, which can be determined by the following formula [7]:

$$Z = \dot{\varepsilon} \exp \frac{Q}{RT} \tag{4}$$

In the formula: Q is the deformation activation energy (J/mol), and R is the gas constant (8.314J•mol-1•K-1).

Take the peak stress data in the strain range and draw the curves at different temperatures, as shown in Figures 3. It can be seen that under different temperature conditions, and are in a linear relationship and are basically parallel to each other. The linear regression analysis results also show that the values obtained by each curve regression are between 0.95696 and 0.99977, and the linear relationship is good.

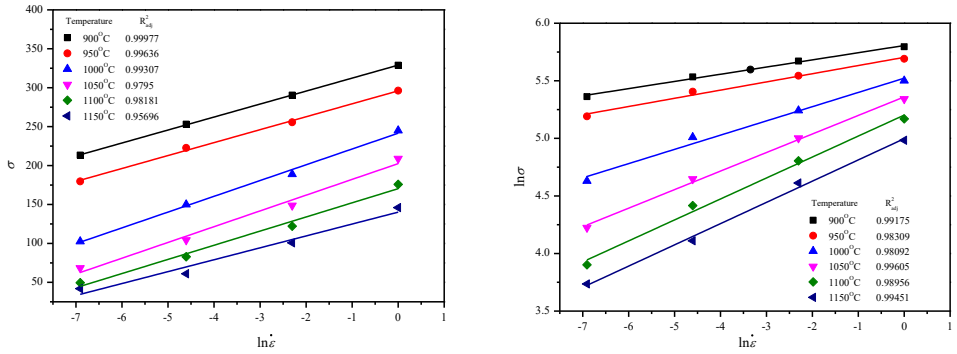

Fig. 3. σ - $\ln \dot{\varepsilon}$ and $\ln\sigma$ - $\ln \dot{\varepsilon}$ Curves at different temperatures

Table 3 shows the slope of each straight line, and the value of 1/β at each temperature is calculated and averaged. The average value of 1/n1 is 0.00736.

Table 3. 1 / β at different temperatures novel titanium aluminum, 1 / n1 values

Temperature (°C)	900	950	1000	1050	1100	1150
$1/\beta$	16.66605	16.6148	20.25767	20.24577	18.16832	15.28239
$1/n_1$	0.06234	0.07113	0.12358	0.16099	0.18205	0.18438

Substituting formula (4) into formula (3) and taking the natural logarithm, we get:

$$\ln[\sinh(\alpha\sigma)] = \frac{1}{n_2} \ln \dot{\varepsilon} - \frac{1}{n_2} \ln A_3 + \frac{Q}{n_2 RT} \tag{5}$$

Substituting the peak stress and temperature values at different strain rates into equation (5), draw the relationship curve between ln[sinh(ασ)] and 1/T, shown in Figure 4. It can be seen from Figure 4 that ln[sinh(ασ)] has a linear relationship with 1/T. Linear regression analysis also shows that under the condition of constant strain rate, the linear regression value R^2_{adj} of ln[sinh(ασ)] and 1/T is 0.96969~0.99548, indicating that ln[sinh(ασ)] has a good linear relationship with 1/T . Calculate the average of the slopes of the straight lines in Figure 4, and get k=12327.21. Similarly, draw ln[sinh(ασ)] and $\ln \dot{\varepsilon}$ the relationship curve,

see Figure 5, and get the average value of n2 to be 5.8711. Deformation activation energy Q=n2kR=601720.9J/mol.

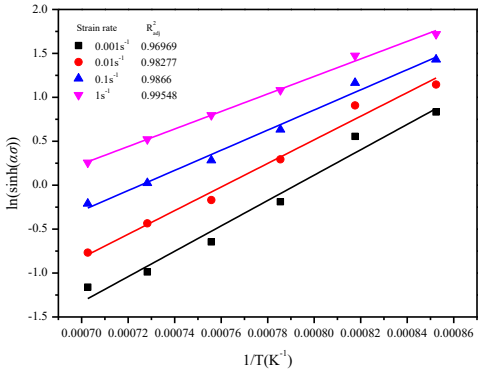

Fig. 4. ln[sinh(ασ)] and 1/T relationship lines

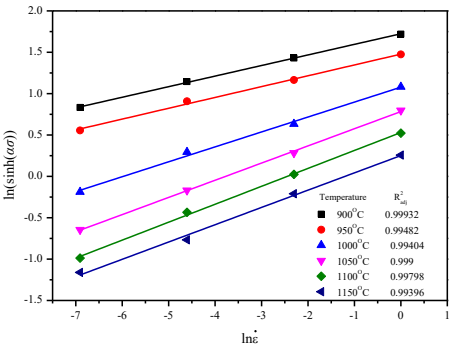

Fig. 5 ln[sinh(ασ)] and $\ln\dot{\varepsilon}$ relationship lines

Take the natural logarithm on both sides of formula (3) and rewrite it into the following form:

$$\ln Z = n\ln\left[\sinh(\alpha\sigma)\right] + \ln A \tag{6}$$

According to the calculated Q value, the Z value under all test conditions is calculated. The relationship between ln[sinh(ασ)] and lnZ is shown in Figure 6. It can be seen from the figure that ln[sinh(ασ)] and lnZ satisfy a linear relationship, and the R^2_{adj} value obtained by linear regression is 0.97583. Therefore, formula (6) can characterize the relationship between stress, deformation temperature and strain rate during high-temperature compression and deformation of new titanium-aluminum materials [8-10].

From the above derivation, the parameters n=4.735 and A=3.117×1012 in formula (6) can be obtained, and then the constitutive equation of the peak stress during the hot compression deformation of the new titanium aluminum material is obtained:

$$\dot{\varepsilon} = 8.38\times10^{21}\ln\left[\sinh(0.00736\sigma)\right]^{5.778343}\exp\left(-601720.9/RT\right) \tag{7}$$

The expression of the Z parameter of the new titanium aluminum material is:

$$Z = \dot{\varepsilon}\exp\left(601720.9/\mathrm{RT}\right) \tag{8}$$

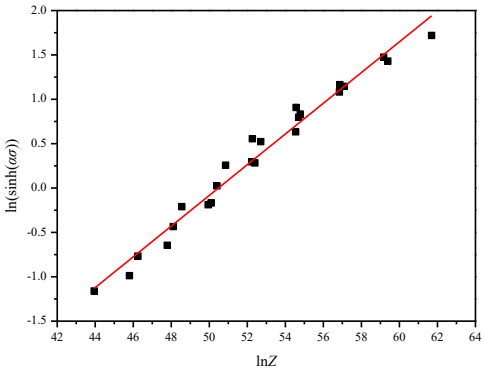

Fig. 6. ln[sinh(ασ)] and lnZ relationship lines

The thermal processing diagram is shown in Figure 7, the shaded area represents the instability zone [11-12]. It can be seen that as the strain increases, the instability zone gradually decreases, and most of them are concentrated in the temperature range below 1000°C.

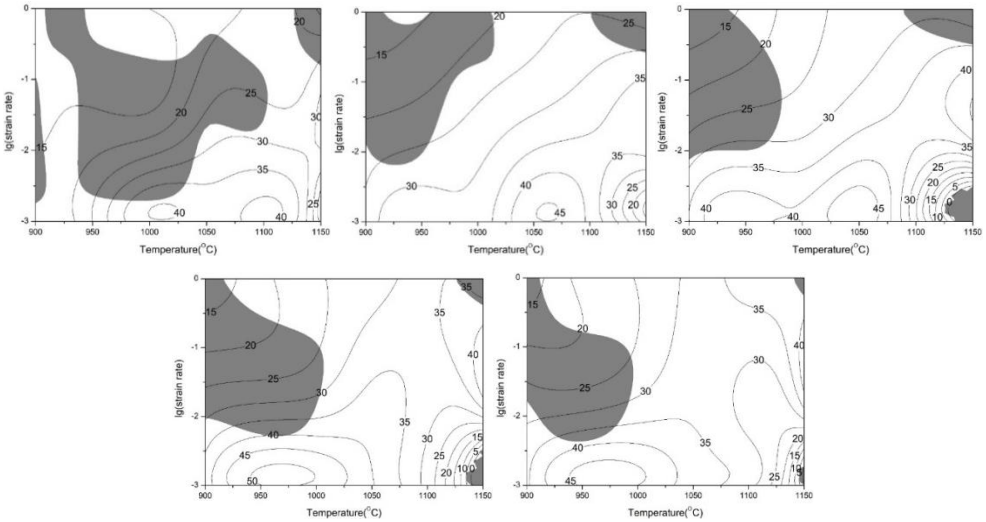

Fig. 7. Thermal processing map

Dynamic softening mechanisms mainly include dynamic recovery (DRV) and dynamic recrystallization (DRX). The obvious difference between the two mechanisms is that the dynamic recrystallization process can cause a significant drop in flow stress. Therefore, the main difference between dynamic recovery type and dynamic recrystallization type high temperature deformation is caused by the dynamic recrystallization process.

When DRX is the main mechanism of high temperature deformation, the flow stress can be expressed as:

$$\sigma = \sigma_{rec} - (\sigma_{sat} - \sigma_{ss}) X_{drx} \left(\varepsilon \geq \varepsilon_c \right) \tag{9}$$

For formula recrystallized volume fraction X_{drx}, and saturated steady flow stress σ_{sat} and flow stress σ_{ss}, respectively. The main mechanism of deformation of the flow stress σ_{rec} DRV.

Thus, the dynamic recrystallized volume fraction X_{drx} can be calculated by the following equation:

$$X_{drx} = \left(\frac{\sigma_{rec} - \sigma}{\sigma_{sat} - \sigma_{ss}} \right) \left(\varepsilon \geq \varepsilon_c \right) \tag{10}$$

σ_{rec} can be calculated by the following formula:

$$\sigma_{rec} = \left[\sigma_{sat}^2 + \left(\sigma_0^2 - \sigma_{sat}^2 \right) e^{-\Omega\varepsilon} \right]^{0.5} \tag{11}$$

In the formula, σ_0 is the yield stress; Ω is the dynamic recovery coefficient; ε is the true strain.

When the true strain is less than ε_c, the main mechanism of high temperature deformation is dynamic recovery. Based on the stress-strain curve, the dynamic recovery coefficient can be calculated by the following formula:

$$\Omega\varepsilon = \ln\left(\frac{\sigma_{sat}^2 - \sigma_0^2}{\sigma_{sat}^2 - \sigma_{rec}^2} \right) \quad \varepsilon_0 \leq \varepsilon \leq \varepsilon_c \tag{12}$$

Figure 8 is a typical work hardening rate curve, σ_0, σ_{sat} and σ_{ss} can be obtained from this graph. The dynamic recovery coefficient can be obtained by linearly fitting $\ln\left[\left(\sigma_{sat}^2 - \sigma_0^2\right)/\left(\sigma_{sat}^2 - \sigma_{rec}^2\right)\right]$ the data with the true strain.

The relationship between the dynamic recrystallization critical strain and the peak strain of the superalloy is generally obtained through the following relationship:

$$\varepsilon_c = 0.85\varepsilon_p \tag{13}$$

Where ε_p is the peak strain.

The material constant nd can be obtained by the linear fitting result between ln[-ln(1-Xdrx)] and ln[(ε-εc)/(ε0.5-εc)].

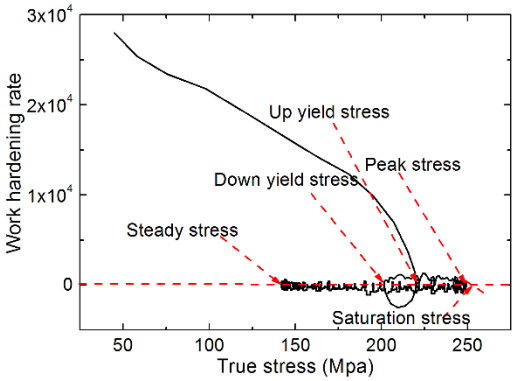

Fig. 8. Work hardening rate curve

Recrystallization volume fraction model:

$$X_d = 1 - \exp\left[-0.4424 \times \left(\frac{\varepsilon - \varepsilon_c}{\varepsilon_p} \right)^{1.1158} \right] \tag{14}$$

$$\varepsilon_p = 0.00095 Z^{0.10667} \tag{15}$$

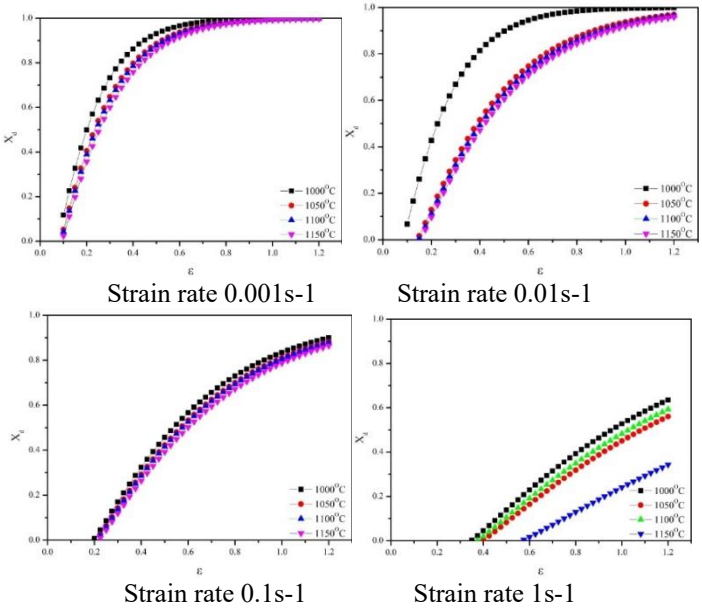

Fig. 9. Recrystallization curve

4 Conclusions

This paper proposes an exploratory study on the preparation of titanium-based superalloys through the Ti+Al+Ti2AlNb three-component hybrid hot press sintering method. Through

the hot press sintering experiment of the mixed powder under different heating and sintering processes, the plastic deformation behavior of the material is carried out on this basis Research, preliminarily discuss the constitutive relationship of the new high-temperature titanium alloy Ti-Al-Nb, establish the hot working map and recrystallization model. The expression of the Z parameter of the new titanium aluminum material is: $Z = \dot{\varepsilon} \exp(601720.9/\mathrm{RT})$, Recrystallization volume fraction model:

$$X_d = 1 - \exp\left[-0.4424 \times \left(\frac{\varepsilon - \varepsilon_c}{\varepsilon_p} \right)^{1.1158} \right] \tag{16}$$

References

[1] Guo J T. Materials Science and Engineering for Superalloys-Superalloy materials and engineering applications[M]. Beijing: Science Press, 2007, 1-91.

[2] Fecht. H, Furrer. D. Processing of Nickel-Base Superalloys for Turbine Engine Disc Applications [J]. Advanced Engineering Materials, 2000, 2: 777-787.

[3] Zhang L, Liu H S, He X B, Din R, Qu X H, Qin M L, Li Z, Zhang G Q. Thermal evolution behavior of carbides and γ′ precipitates in FGH96 superalloypowder[J]. Materials Characterization, 2012, 67: 52-64.

[4] Sherby O D, Wadsworth J. Superplasticity—Recent advances and future directions [J]. Progress in Materials Science, 1989, 33: 169-221.

[5] Kaibyshev O A. Fundamental aspects of superplastic deformation[J]. Materials Science and Engineering A, 2002, 324: 96-102.

[6] Rabinovich M K, Trifonov V G. Dynamic grain growth during superplastic deformation [J]. ActaMaterialia, 1996, 44: 2073-2078.

[7] Feltham P. Grain growth in metals[J]. ActaMetallurgica, 1957, 5: 97-105.

[8] Bulatov V V, Reed B W, Kumar M. Grain boundary energy function for fccmetals[J]. ActaMaterialia, 2014, 65: 161-175.

[9] Sallez N, Boulnat X, Borbely A, et. In situ characterization of microstructural instabilities: Recovery, recrystallization and abnormal growth in nanoreinforced steel powder[J]. ActaMaterialia, 2015, 87: 377-389.

[10] Darnbrough J E, Flewitt P E J. Growth of abnormal planar faceted grains in nanocrystalline nickel containing impurity sulphur [J]. ActaMaterialia, 2014, 79: 421-433.

[11] Luan Z J, Wang F, Yao D W, Huang L Y, Meng L. Effect of interface energy on abnormal grain growth in pyrite films prepared by sol-gel method[J]. Materials Research Bulletin, 2011, 46: 1577-1581.

[12] Ma F, Zhang J M, Xu K W. Surface-energy-driven abnormal grain growth in Cu and Ag films[J]. Applied Surface Science, 2005, 242: 55-61.